Finite Element Analysis of A Self Expanding Nitinol Cardiovascular Stent

Finite Element Analysis Project (MEP55B10)

Conall Daly[1] Eoghan O'Doherty[2]

January 3, 2023

1 Introduction

Cardiovascular diseases are the leading cause of death globally, with an estimated 17.9 million people killed each year [1]. On of the most common cardiovascular diseases is atherosclerosis. This is characterised by a build up of plaque on the walls of arteries as shown in Figure 1 which can lead to constricted blood flow and if left untreated, a blocked artery.

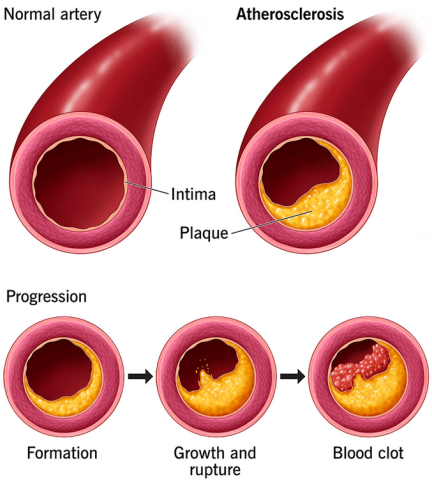

Figure 1: Development of plaque in arteries leading to atherosclerosis [2].

The most successful treatment of atherosclerosis has been through the deployment of intravascular stents which are used to restore patency [3]. There are two main types of stents:

Balloon Expandable Stents
Made of a ductile material which is expanded upon insertion into the diseased artery.

Self Expanding Stents
Crimped down to a smaller diameter than it's manufactured diameter for insertion into the artery and then uncrimped allowing it to expand to support the arterial wall.

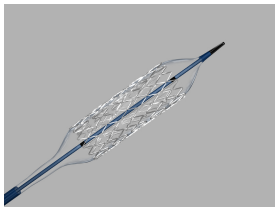

(a) Cook Medical Formula 418® balloon expanded stent [4].

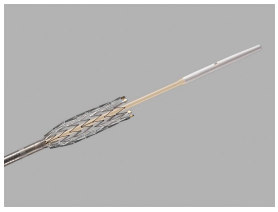

(b) Cook Medical Zilver 635® self expanded stent [5].

Figure 2: Visual comparison of balloon expanded and self expanded stent designs.

Self expanding stents require exotic properties which result in a material that requires more force to compress than it does to expand resulting in support of the arterial wall. These material properties are found in

the Nitinol alloy developed in the late 1950's to early 1960's at the U.S. Naval Ordnance Laboratory in Maryland.

Designing components with Nitinol requires a large amount of experience with the material and geometrical constraints are another factor which complicates finding an optimum design for a use case. This is where finite element analysis (FEA) can enhance the design skills of an engineer and achieve optimum design of mechanical components.

This report aims to use FEA simulate a self expanding Nitinol stent using the geometry shown in Figure 3a as a baseline design and examining how modifying the dimensions shown in Figure 3b affects the the long term radial force imparted to a patients arterial wall during normal operation and the fatigue life of the stent.

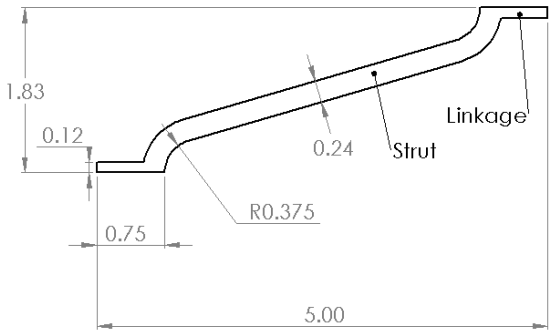

(a) Original geometry for stent.(Thickness = 0.24mm)

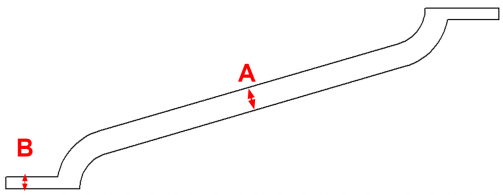

(b) Two dimensions to be modified for design analysis, strut thickness (A) and link thickness (B).

Figure 3: Stent schematic and geometric parameters to be modified.

2 Methodology

2.1 Material Model

Nitinol is a superelastic alloy composed of Titanium and Nickel. This allows the material to undergo large deformations but return to it's original shape once the external load has been removed.

Nitinol also exhibits a property known as shape memory due to the two temperature dependent crystalline structures present in the material, Martensite and Austenite. This allows the Nitinol to undergo deformation at one temperature and stay deformed when the external force has been removed. Then by heating the material above its transformation temperature (75 $^{\circ}$C) it will return to its original shape.

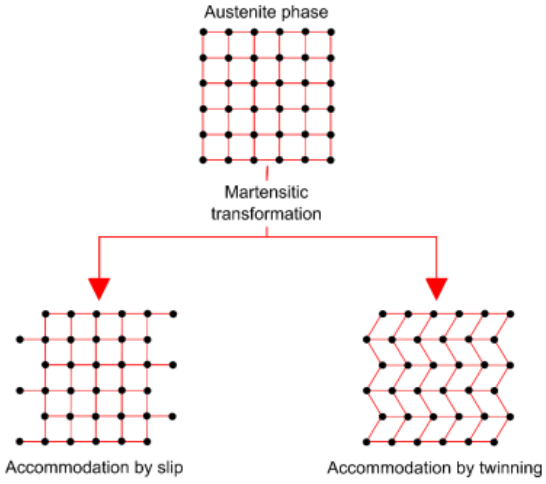

Figure 4: Slip versus twinning mechanism in Martensitic transformations [6].

The unusual properties of Nitinol are mainly attributed to the twinning mechanism which results in atomic bonds in the metal being rotated by a partial atomic spacing rather than slipping and forming new bonds, shown in Figure 4.

When the Nitinol is Martensitic the bonds are free to move around without breaking giving the perception they are being deformed. When the Nitinol transforms to

Austenite they reform back into a solid cubic structure as none of the bonds have broken. By maintaining these bonds they can spring back to their original configuration, giving the material it's so called "shape memory".

The two metallic crystalline phases, Austenite and Martensite, introduced partial atomic spacing of the twinning mechanism result in Nitinols unusual super-elastic property and hysteresis in it's stress-strain characteristic as shown in Figure 5.

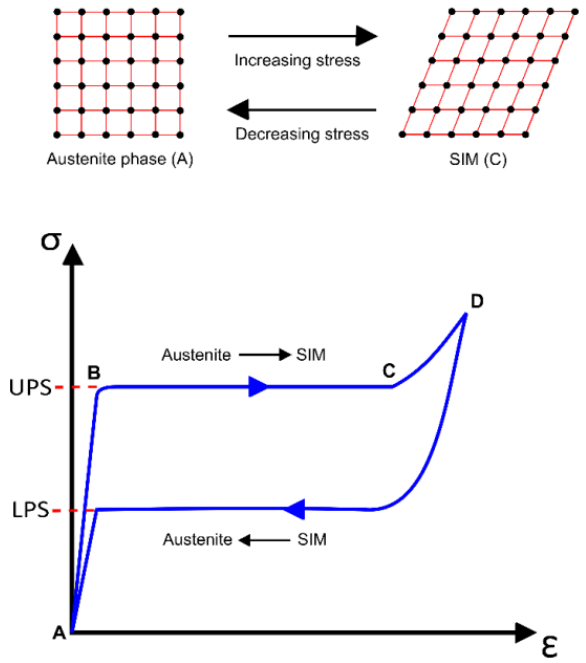

Figure 5: Stress Induced Martensite (SIM), upper plateau strength/stress (UPS) and lower plateau strength/stress (LPS). During initial loading the Austenite phase exhibits typical elastic deformation (A→B) up until the UPS is reached. Once the UPS has been reached an isostress condition is observed (B→C) as the cubic Austenite structure shears into detwinned SIM, followed by the elastic deformation of the detwinned SIM structure (C→D). Just as for the thermally induced phase transformation, the formation of SIM is reversible. During unloading (D→A) elastic strain is recovered and the SIM transforms back into the parent Austenite phase [6].

For simulating Nitinol an approximation of the constituitve model is used by entering discrete points along the stress-strain curve and using a linear interpolation between these points. The particular emprically derived points used for this study are shown in Table 1.

Table 1: Nitinol material properties.

Elastic Properties	
Young's Modulus	40000 MPa
Poisson's ratio	0.33
Super-Elastic Properties	
Martensitic Young's Modulus	30000 MPa
Martensitic Poisson's ratio	0.33
Transformation Strain	0.053
Start of Transformation (Loading)	417 MPa
End of Transformation (Loading)	450 MPa
Start of Transformation (Unloading)	136 MPa
End of Transformation (Unloading)	96 MPa
Start of Transformation in Compression (Loading)	591 MPa
Reference Temperature	0 °C
Loading	6 °C
Unloading	6 °C

To verify the material properties were correct for the stent, a single element cube was modelled and loaded with a pressure of 430 MPa and then unloaded. as seen in Figure 6.

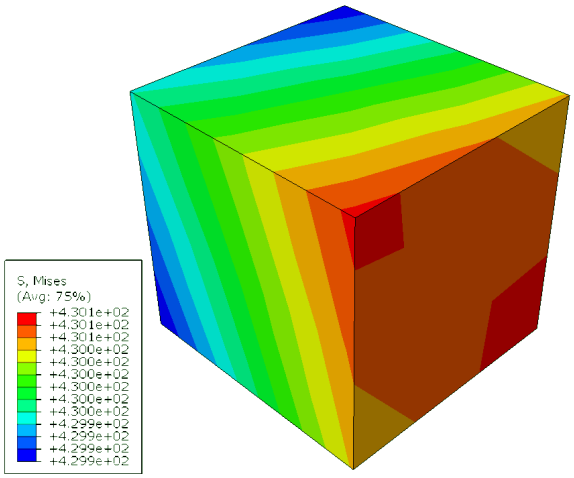

Figure 6: Nitinol cube uniaxial stress visualisation in fully loaded state.

Figure 7 shows that this sample case exhibits the hysteresis present in Nitinol and that it will model it correctly in so far that we have used reasonable assumptions for the temperature range for our use case.

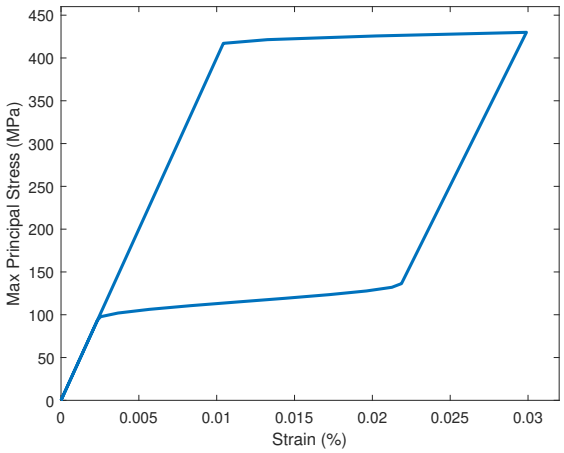

Figure 7: Nitinol uniaxial test stress-strain curve.

2.2 Geometry Changes

Testing the model involved changing two aspects of the models original geometry in order to see the overall effect this would have on the results and compare it to the baseline geometry.

Figure 3b shows the elements on the geometry where the dimensions were modified. The first case seen in Figure 8b involved doubling the original strut thickness to 0.48mm. The second case seen in Figure 8c uses and increased link thickness of 0.24mm with the third and final case seen in Figure 8d uses a decreased strut thickness of 0.12mm.

The method used for the simulation of the original geometry was applied for the other cases in order to compare how the geometry modifications would impact the stent and draw conclusions about the geometry.

(a) Original geometry for stent.

(b) Stent geometry with increased strut thickness.

(c) Stent geometry with increased link thickness.

(d) Stent geometry with decreased strut thickness.

Figure 8: Stent geometry modifications for parametric design study.

2.3 Element Selection

For the stent an incompatible non-standard element **C**ontinuum, **3**-**D**imensional, **8** Node,

Reduced/**I**ncompatible (C3D8I) was used. C3D8I elements have additional DoF's to capture bending better and reduce shear-locking.

An online analysis [7] compared C3D8R (standard element, reduced integration), C3D8 (standard element) and C3D8I elements for beam bending. In this study the simple example of a beam deflecting 2 mm was compared in FEA for the three elements. C3D8R over predicted 2.664 mm on the coarsest mesh, C3D8 under predicted deflection as 1.310 mm on the coarsest mesh and C3D8I under predicted the delfection as being 1.962 mm. Only 5% error on a pretty coarse mesh for such a small increase in computation is another reason why the C3D8I element was chosen.

For the crimper a 4-noded quadrilateral surface element with reduced integration was used for the mesh, **S**ur**F**ace, **M**embrane, **3**-**D**imensional, **4** Node, **R**educed (SFM3D4R). This element was chosen for simplicity as it was only to be used for contact modelling purposes.

2.4 Boundary Conditions

Boundary conditions for the model were defined relative to a cylindrical coordinate system (r, θ, z) so displacements are defined as U_r, U_θ, U_z.

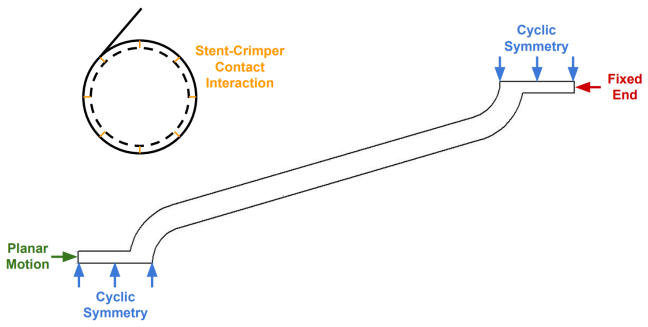

Figure 9: Application of boundary conditions to stent geometry.

Good boundary conditions constrain the geometry in such a way that it is allowed to deform realistically while keeping it fixed in place giving adequate assumptions to make the stiffness matrix solvable. The boundary conditions applied to the stent and between the stent and the crimper are shown in Figure 9.

To enforce cyclic symmetry for the stent a value of $U_\theta = 0$ is applied to the two ends shown in light blue in Figure 9. To constrain the stent in the z-direction a boundary condition of $U_z = 0$ was applied to the end shown in red in Figure 9. In order to creating axial symmetry, the free end had it's motion constrained to the z-plane using an equation constraint on the end shown in green in Figure 9.

To model the force exerted by the crimper on the stent a rigid body "hard contact" normal interaction was defined between the two geometries. This interaction works based on a penalty method by applying a reaction force to the stent based on how far it intersects into the crimper geometry (a method heavily used in multi-body simulation).

Three loading conditions modelling crimping, expansion and fatigue loading of the stent were defined, these were modelled by simply a displacement boundary condition to the crimper of $U_r = -1.5, U_r = -0.5$ and $U_r = -1.0$ for each respective load case.

2.5 Non-Linearities

There are a number of non-linearities in the model which affect it's complexity:

Large Deformations

The stent undergoes a large deformation being compressed form 7mm down to 4mm during the crimping stage. Large deformations resulting in large non-linearities between simulation states and as such require a small enough time step to allow the solver to remain stable.

Material Model

The two metallic phases of the Nitinol mean that the Young's Modulus varies depending on the stress state of the

component.

Nitinol's material properties have a high dependency on temperature, this is not taken into account in this model using a reference temperature of 0 $^{\circ}$C.

Contact Interaction
The contact between the stent and the crimper is a large source of non-linearity in the model due to the complexity of contact interactions. The reaction force between two interacting components is a function many factors such as surface roughness and friction. While a simpler model is used here by modelling the interaction as a hard rigid contact with a penalty function this still is quite complex.

3 Results & Discussion

3.1 Stress Visualisation

Plotting stress contours on the surface of the stent geometry in Figure 10 indicate regions of high stress concentrations for each of the three load cases.

The crimping process resulted in the highest stresses experienced by the stent with a value of around 710 MPa. This may be uncomfortably close to the ultimate strength of Nitinol (895 MPa for fully annealed Nitinol [8]) depending on the factor of safety defined for the design and may indicate the need for further material processing (such as work hardening) to be applied to the Nitinol to increase it's strength.

Stress visualisation also shows that stress concentrations are highest on the inner bend of the fork geometry. This information aided the decision for the design changes indicating that the design would benefit from the addition of material towards the bend connecting each strut to reduce stresses here. As will be discussed later, rather counter-intuitively, the opposite turned out to be true with a reduction in material here resulting in a lower stress.

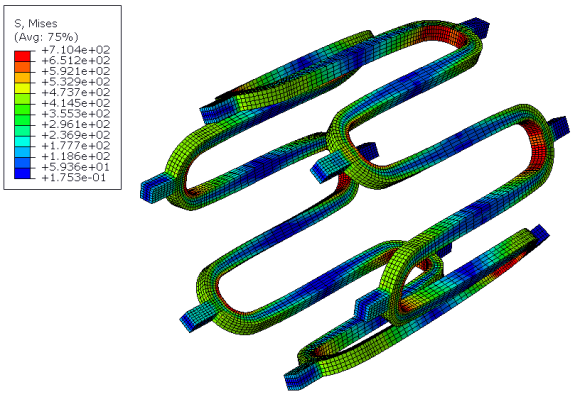

(a) Stress state at the end of the crimping phase.

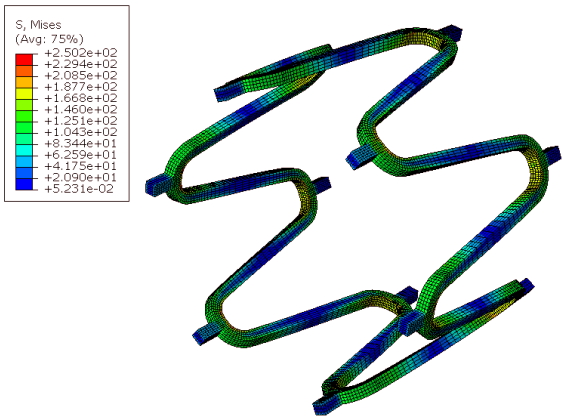

(b) Stress state at the end of the expansion phase.

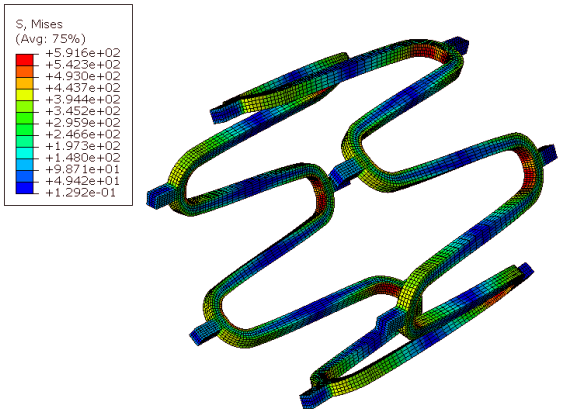

(c) Stress state at the end of the fatigue phase.

Figure 10: Stress state for the three phases of deployment of the original stent geometry.

3.2 Arterial Radial Force

Stents require careful design to achieve a certain force-diameter characteristic that suitably supports a patients arterial wall while not exerting so much outward force as to cause discomfort for the patient.

The long term radial force exerted by a stent during it's lifetime is termed chronic outward force (COF), early studies believed that COF was beneficial in preventing stent collapse but recently it has been shown that high COF could contribute to inflammation and neointimal proliferation in the vessel [9]. In general the COF required is determined by a clinician by over sizing a stent (implanting a stent with a bigger diameter than the artery) but it is up to the stent designer to provide a low COF with a flat response across the operating diameters. The stent studied here is 1mm oversized for the simulated artery.

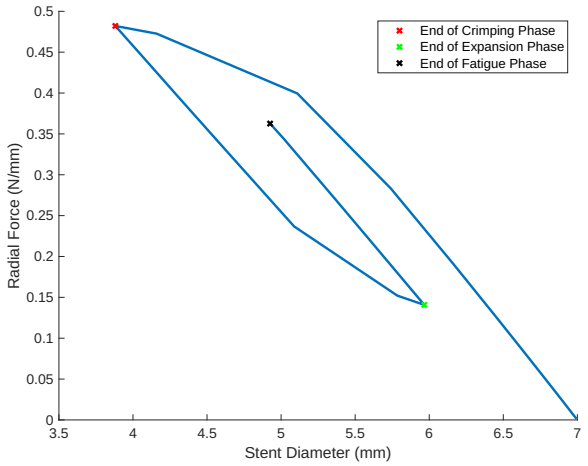

Figure 11: Original geometry radial force vs. stent diameter.

The radial force exerted by the baseline stent as it transitions between the three load cases is shown in Figure 11. The COF is characterised by the line connecting the expansion phase to the end of the fatigue phase with the stent transitioning between these two points over it's lifetime.

The original stent design exhibited a COF of between 0.15-0.35 N/mm. To have a reference to compare to empirical radial force results for a laser-cut Nitinol SE stent with a nominal 10 mm diameter were obtained from Duerig et al. 2000 [10]. These results are plotted against the results obtained from the FEA model in Figure 12

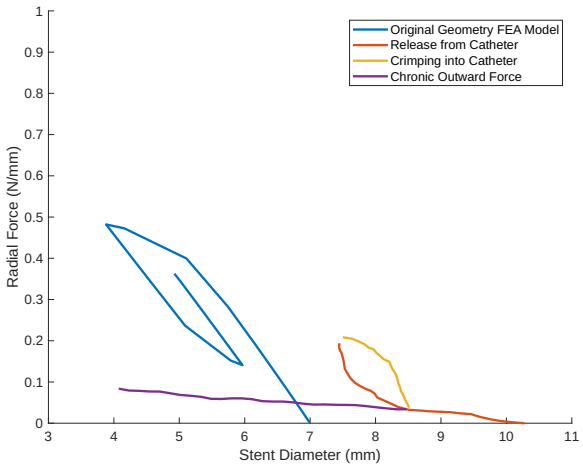

Figure 12: FEA radial force vs. stent diameter compared against empirically measured values.

From this comparison the FEA geometry exerts a COF of almost double that of the stent in Duerig which had a COF of 0.035 N/mm and maintained an almost flat COF response across it's operating diameters (8-9 mm). In general the original geometry exhibits a far stiffer force characteristic than the stent in Duerig, this may be due to the hard contact characteristic enforced between the crimper and stent which is a crude approximation to the actual deformation behaviour of a human artery.

Assuming that the FEA model is correct (it would really need to be validated with experimental modelling and measurement) the model could benefit from changes to it's geometry to reduce it's COF. Initially the fatigue results were also examined alongside the COF results and it was found that the original geometry was on the boundary of failure for cyclic strain results and so increases in strut and link geometry were examined to see if they would result in a longer fatigue life for the stent.

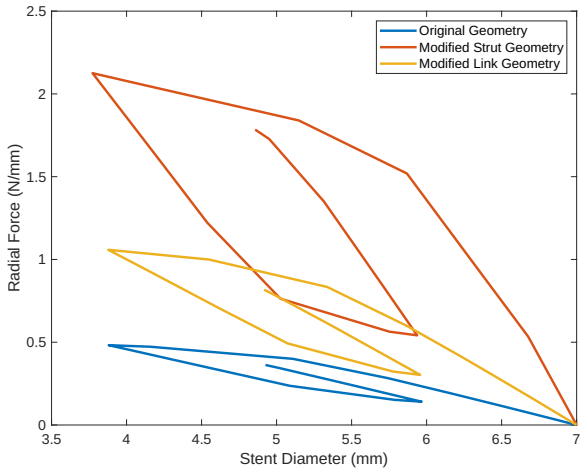

Figure 13: Modified strut geometry radial force vs. stent diameter graph.

As shown in Figure 13 both of these geometries resulted in a stiffer response of the stent and a higher COF. Interestingly doubling the strut geometry had the largest effect on the radial force compared to doubling the size of the link geometry, with a doubling in the size of the strut geometry resulting in a four fold increase of the exerted radial force.

The higher COF (and poor fatigue, life discussed later) indicated that reducing the geometry of the stent might achieve a better design. Halving the strut size resulted in the radial force results shown in Figure 14.

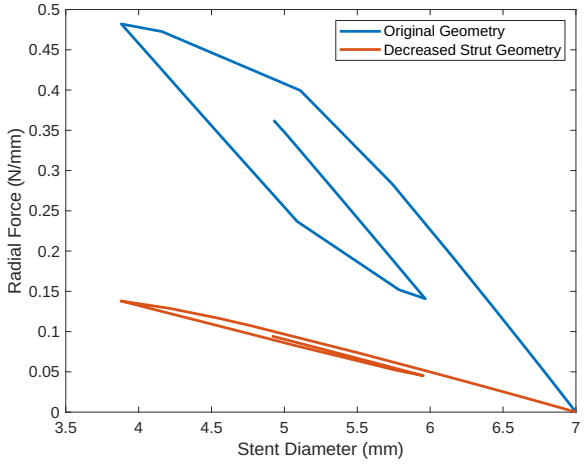

Figure 14: Modified strut geometry radial force vs. stent diameter graph.

As can be seen this change results in a much lower COF between 0.05-0.1 N/mm and much smaller change in COF across it's operating range.

Empirical COF data was obtained for a number of commercially available stents from Wressenger et al. 2017 [9] to compare the FEA designs against real world stent performance shown in Figure 15.

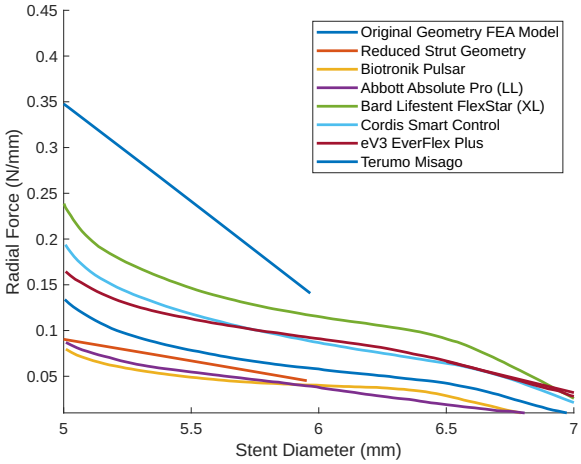

Figure 15: FEA geometry COF results compared against performance of commercially available stents.

The original geometry performs quite poorly with a COF of almost double that of the worst performing commercially available stent, the Bard Lifestent FlexStar (XL). The reduced strut size geometry performs almost on par with the two best preforming stents, the Abbott Absolute Pro (LL) and the Biotronik Pulsar.

It's worth noting the almost perfectly linear COF of the FEA models compared to the small nonlinearity in the response of the physical stents close to 5mm diameter. This may indicate that better contact modelling is required for capturing the deformation of the artery.

3.3 Fatigue Failure

Determining whether a design will fail from cyclical strain requires the calculation of the following values:

$$\textbf{Mean Strain} = \frac{\epsilon_{t=0}^{max} + \epsilon_{t=1}^{max}}{2} \qquad (1)$$

$$\textbf{Alternating Strain} = \frac{|\epsilon_{t=0}^{max} - \epsilon_{t=1}^{max}|}{2} \quad (2)$$

The two time values $t = 0$ and $t = 1$ denote the beginning and the end of the fatigue loading step in the simulation respectively.

Fatigue data based on cyclic strain values was obtained from Pelton et al. 2011 [11]. In Figure 16 the mean and alternating strain for each geometry are plotted against the failure boundary determined by Pelton.

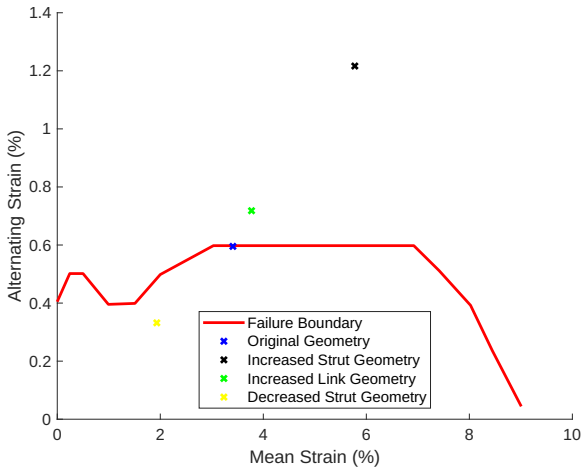

Figure 16: Three stent geometries compared against empirical fatigue failure data.

As can be seen the original geometry presents an edge case as it lies right on the failure boundary. The increased strut and link size both resulted in failure of the stent. From the fatigue life S-N diagram in Pelton they can be expected to last between 10^4-10^5 cycles (a human heart beats 35 million times per year, original and increased size geometry would not last even a year). It should be made clear that Pelton noted that there was insufficient experimental data between mean strains of 3% and 7% and so the likelihood of failure for these cases should be taken with a degree of scepticism.

Rather counter intuitively the reduced strut size resulted in a longer fatigue life and a lower maximum principal stress compared to the original geometry (the original geometry had a max.principal stress of 480 MPa at the end of the fatigue phase and the reduced strut geometry had a max.principal stress of 411 MPa). This could be because an increase in the size of whole structure (increasing strut) size increases overall stiffness leading to higher reaction forces which leads to higher stresses pushing the Nitinol into the more ductile region as the Austenite structure shears into the detwinned stress induced Martensite, which allows for a large strain for relatively small changes in stress. This theory coincides with the stress range between the two designs with 411 MPa being at the start of the upper plateau strength region for the Nitinol and 480 MPa being well within the elastic region of the detwinned stress induced Martensitic structure.

4 Mesh Independence Study

Mesh convergence was determined by measuring how max. principal stress at the end of crimping stage varied with a reduction in mesh size.

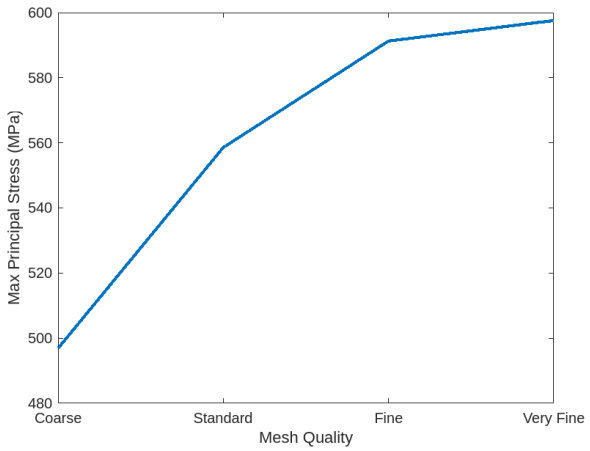

Figure 17: Mesh quality versus max. principal stress (mesh quality labels on x-axis refer to labels on more detailed mesh quality metrics in Appendix B).

As seen in Figure 17 the solution shows reasonable convergence to a max. principal stress value of around 600 MPa. For computational efficiency the fine mesh was used for all simulations.

5 Conclusions

The analysis presented here relies heavily on the assumption that the FEA model is right. This can be determined through verfication (did we solve the right model i.e. assumed correct boundary conditions and static loading) and validation (how does it compare to experimental results?).

Taking the FEA simulation as accurate we have gained some valuable insight into how geometric changes affect the mechanical response of the stent, something that would have been quite complex and laborious with hand calculations (though these would be very useful for verifying FEA simulations). However these changes need to take into account physical constraints, for example the smaller strut size indicated as a better design in the analysis above may be very difficult or impossible to manufacture due it's small size.

One very important material constraint not addressed in the Nitinol material model is impurities. Theoretically, Nitinol is strictly a mixture of Nickel and Titanium but in reality impurities such as Carbon and Oxygen can be dissolved into the metal during smelting processes. These result in Carbide and Oxide impurities of a different chemical composition to that of the base metal, such as the oxide, Ti_2NiOx, inclusion shown in Figure 18.

These inclusions can act as initiation sites for fatigue cracks and can even promote corrosion. While there are strict limits to these in manufactured Nitinol they will play a role in determining the fatigue life of a component as seen in this analysis and so are worth taking into consideration.

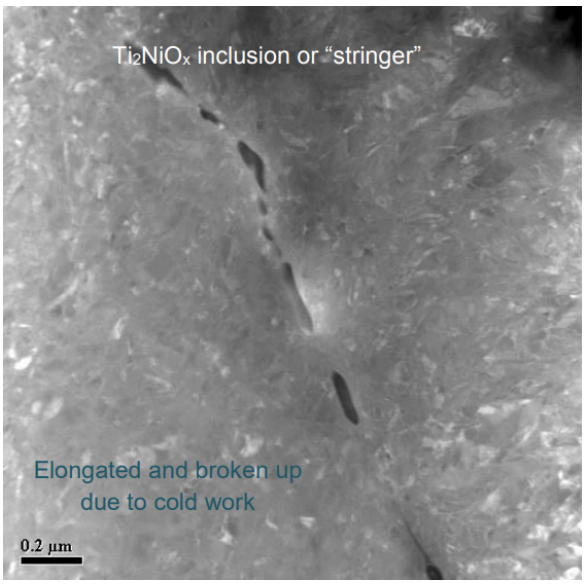

Figure 18: Nitinol inclusion capture using a Scanning Electron Microscope (SEM) [6].

References

[1] *World Health Organisation | Cardiovascular Diseases*. URL: https://www.who.int/health-topics/cardiovascular-diseases (visited on 12/17/2022).

[2] *Cleveland Clinic | Atherosclerosis: Arterial Disease*. URL: https://my.clevelandclinic.org/health/diseases/16753-atherosclerosis-arterial-disease (visited on 12/19/2022).

[3] C. Lally, F. Dolan, and P. J. Prendergast. "Cardiovascular Stent Design and Vessel Stresses: A Finite Alement Analysis". In: *Journal of Biomechanics* 38.8 (Aug. 2005), pp. 1574–1581. DOI: 10.1016/j.jbiomech.2004.07.022.

[4] *Cook Medical | Formula 418® Biliary Balloon-Expandable Stent*. URL: https://www.cookmedical.com/products/di_forb4_webds/ (visited on 12/19/2022).

[5] *Cook Medical | Zilver 635® Biliary Self-Expanding Stent*. URL: https://www.cookmedical.com/products/esc_zilbs635/ (visited on 12/19/2022).

[6] Memry Corporation SAES Group. *Introduction to Nitinol*. 2017.

[7] Bill Webster. *Hourglassing and Shear Locking - What Are They And Why Does It Matter?* Mar. 2021. URL: https://www.fidelisfea.com/post/hourglassing-and-shear-locking-what-is-it-and-why-does-it-matter (visited on 12/23/2022).

[8] *Johnson Matthey | Nitinol technical properties*. URL: https://matthey.com/products-and-markets/other-markets/medical-components/resource-library/nitinol-technical-properties (visited on 12/22/2022).

[9] Alexander Wressnegger, Alexandra Kaider, and Martin A. Funovics. "Self-expanding nitinol stents of high versus low chronic outward force in de novo femoropopliteal occlusive arterial lesions (BIOFLEX-COF trial): study protocol for a randomized controlled trial". In: *Trials* 18.1 (Dec. 2017). DOI: 10.1186/s13063-017-2338-0.

[10] T. W. Duerig, D. E. Tolomeo, and M. Wholey. "An overview of superelastic stent design". In: *Minimally Invasive Therapy and Allied Technologies* 9.3-4 (Jan. 2000), pp. 235–246. DOI: 10.1080/13645700009169654.

[11] A. R. Pelton. "Nitinol Fatigue: A Review of Microstructures and Mechanisms". In: *Journal of Materials Engineering and Performance* 20.4-5 (July 2011), pp. 613–617. DOI: 10.1007/s11665-011-9864-9.

Appendix A Stent Mesh Visualisations

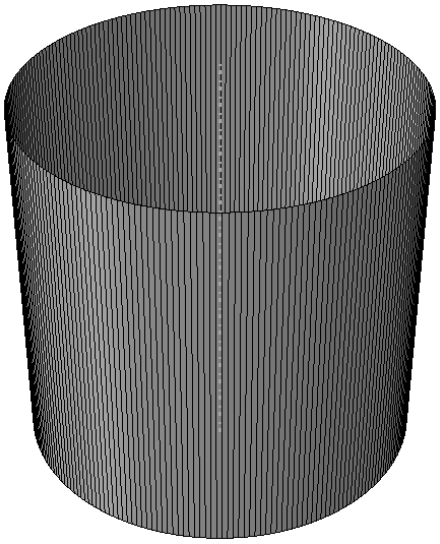

Figure 19: Crimper mesh.

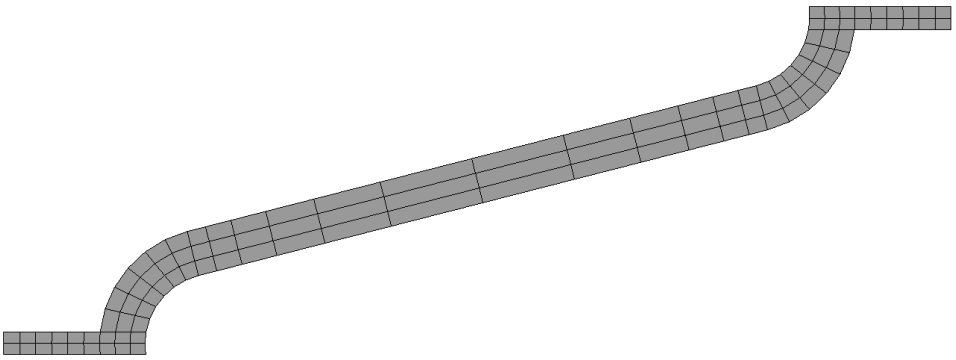

Figure 20: Coarse stent mesh.

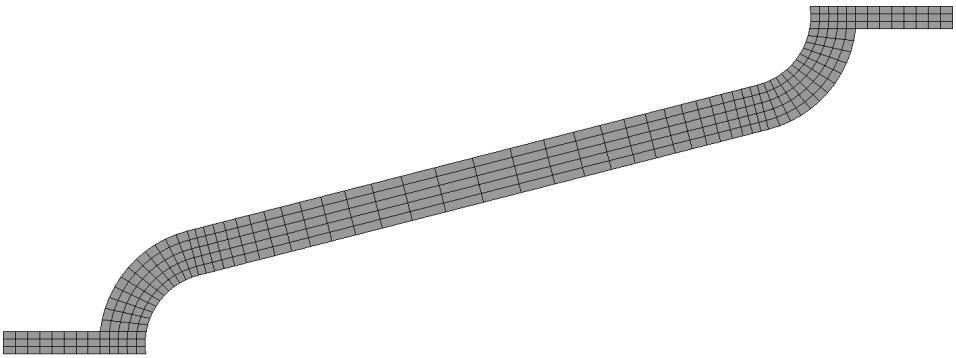

Figure 21: Standard stent mesh.

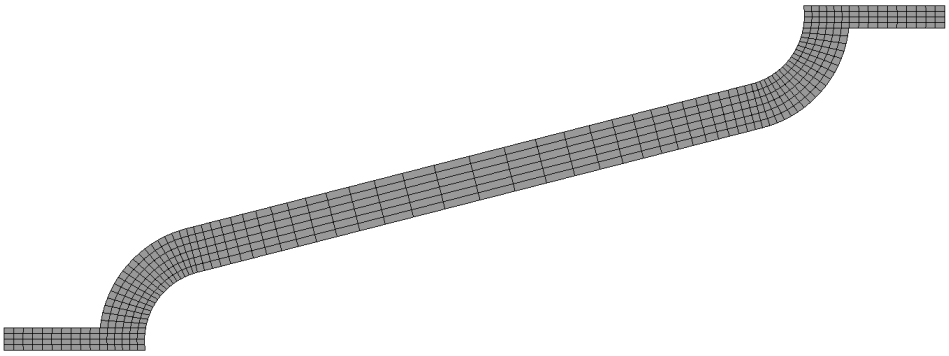

Figure 22: Fine stent mesh.

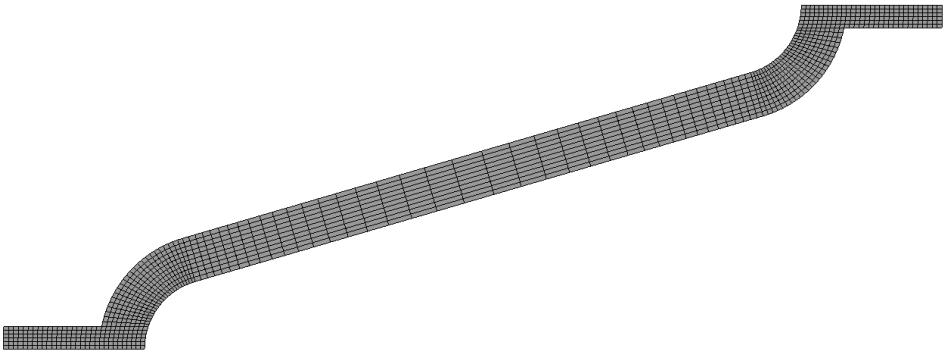

Figure 23: Very Fine stent mesh.

Appendix B Stent Mesh Metrics

Mesh Independence Study Data							
Job	**Average Min. Angle (Degrees)**	**Average Max. Angle (Degrees)**	**Average Aspect Ratio**	**Average Min. Edge Length**	**Average Max. Edge Length**	**Number of Elements**	**Max Principal Stress (MPa)**
Coarse	85.61	94.58	2	0.0729	0.1500	624	496.896
Standard	87.08	93.04	1.76	0.0453	0.0808	1392	558.583
Fine	86.88	93.24	2.14	0.0347	0.0746	2144	591.287
Very Fine	86.52	93.62	1.97	0.0152	0.0439	4233	597.581